Title

Bile acid sequestration reverses liver injury and prevents progression of nonalcoholic steatohepatitis in Western diet–fed mice

Journal

Journal of Biological Chemistry, 295(14)

ISSN

0021-9258

Authors

Takahashi, Shogo
Luo, Yuhuan
Ranjit, Suman
et al.

Publication Date

2020-04-01

DOI

10.1074/jbc.ra119.011913

Peer reviewed

Bile acid sequestration reverses liver injury and prevents progression of nonalcoholic steatohepatitis in Western diet–fed mice

Received for publication, November 13, 2019, and in revised form, February 13, 2020 Published, Papers in Press, February 19, 2020, DOI 10.1074/jbc.RA119.011913

Shogo Takahashi[‡§1], Yuhuan Luo[¶1], Suman Ranjit[‡‖1], Cen Xie[§1], Andrew E. Libby[‡1], David J. Orlicky[**], Alexander Dvornikov[‖], Xiaoxin X. Wang[‡], Komuraiah Myakala[‡], Bryce A. Jones[‡‡‡], Kanchan Bhasin[‡], Dong Wang[¶], James L. McManaman[§§¶¶], Kristopher W. Krausz[§], Enrico Gratton[‖], Diana Ir[¶], Charles E. Robertson[¶], Daniel N. Frank[¶], Frank J. Gonzalez[§], and Moshe Levi[‡2]

From the Departments of [‡]Biochemistry and Molecular & Cellular Biology and [‡‡]Pharmacology and Physiology, Georgetown University, Washington, D.C., 20057, the Departments of [**]Pathology, [¶]Medicine, [§§]Division of Reproductive Sciences, and [¶¶]Graduate Program in Integrated Physiology, University of Colorado Anschutz Medical Campus, Aurora, Colorado 80045, the [‖]Department of Biomedical Engineering, Laboratory for Fluorescence Dynamics, University of California at Irvine, Irvine, California 92697 , and the [§]National Cancer Institute, National Institutes of Health, Bethesda, Maryland 20892

Edited by Jeffrey E. Pessin

Nonalcoholic fatty liver disease is a rapidly rising problem in the 21st century and is a leading cause of chronic liver disease that can lead to end-stage liver diseases, including cirrhosis and hepatocellular cancer. Despite this rising epidemic, no pharmacological treatment has yet been established to treat this disease. The rapidly increasing prevalence of nonalcoholic fatty liver disease and its aggressive form, nonalcoholic steatohepatitis (NASH), requires novel therapeutic approaches to prevent disease progression. Alterations in microbiome dynamics and dysbiosis play an important role in liver disease and may represent targetable pathways to treat liver disorders. Improving microbiome properties or restoring normal bile acid metabolism may prevent or slow the progression of liver diseases such as NASH. Importantly, aberrant systemic circulation of bile acids can greatly disrupt metabolic homeostasis. Bile acid sequestrants are orally administered polymers that bind bile acids in the intestine, forming nonabsorbable complexes. Bile acid sequestrants interrupt intestinal reabsorption of bile acids, decreasing their circulating levels. We determined that treatment with the bile acid sequestrant sevelamer reversed the liver injury and prevented the progression of NASH, including steatosis, inflammation, and fibrosis in a Western diet–induced NASH mouse model. Metabolomics and microbiome analysis revealed that this beneficial effect is associated with changes in the microbiota population and bile acid composition, including reversing microbiota complexity in cecum by increasing *Lactobacillus* and decreased *Desulfovibrio*. The net effect of these changes was improvement in liver function and markers of liver injury and the positive effects of reversal of insulin resistance.

Nonalcoholic fatty liver disease (NAFLD)[3] is rapidly increasing in prevalence in the 21st century, and it is a leading cause of chronic liver disease that can lead to end-stage liver diseases, including cirrhosis and hepatocellular cancer. Despite this worsening epidemic, an effective pharmacological treatment has not been developed. Novel therapeutic approaches are required to prevent and decreases the progression of NAFLD and its aggressive form, nonalcoholic steatohepatitis (NASH) (1, 2). The liver is a key metabolic organ exposed to high levels of intestinal products through portal vein and systemic circulation. An altered microbiota (*i.e.* "dysbiosis") may lead to increased intestinal permeability, amplifying many of these gut-derived effects (3). The changes in specific microbial products, secondary to altered gut microbiota composition, and the changes in intestinal permeability and function can affect hepatic structure and function, further increasing the risk of NASH. Patients with NASH have a higher prevalence of microbial dysbiosis. Human studies further document that NASH patients have a less complex gut microbiota than that of healthy subjects (4, 5).

This work was supported by National Institute of Aging Grant AG049493 (to M. L.), National Institute of Diabetes and Digestive and Kidney Diseases Grant 116567 (to M. L.), National Institutes of Health Grants 2R01HD45965 and R01-HD075285 (to J. L. M.), Colorado Clinical and Translational Sciences Institute/National Institutes of Health Grant TL1-TR001081 (to A. E. L.), and National Institutes of Health Grants P50GM076516 and P41GM103540 (to S. R., A. D., and E. G.). This work was also supported by funds from the Gastrointestinal and Liver Innate Immunity Program of the University of Colorado School of Medicine (to D. N. F., D. I., and C. E. R.) and American Heart Association Postdoctoral Fellowships 19POST34430001 (to A. E. L.) and 19POST34381041 (to K. M.). The authors declare that they have no conflicts of interest with the contents of this article. The content is solely the responsibility of the author and does not necessarily represent the official views of the National Institutes of Health.

This article contains supporting text, Table S1, and Figs. S1–S3.

[1] These authors contributed equally to this work.

[2] To whom correspondence should be addressed: Biochemistry and Molecular & Cellular Biology, Georgetown University 3900 Reservoir Rd., Basic Science 353, Washington, D. C., 20057. Tel.: 202-687-9296 E-mail: Moshe.Levi@georgetown.edu.

[3] The abbreviations used are: NAFLD, nonalcoholic fatty liver disease; NASH, nonalcoholic steatohepatitis; LF, low-fat; WD, Western diet; BAS, bile acid sequestration or bile acid sequestrant; FXR, farnesoid X receptor; H&E, hematoxylin and eosin; CARS, coherent anti-Stokes Raman scattering; PSR, Picro Sirius Red; PCA, principal component analysis; LCA, lithocholic acid; ESI, electrospray ionization; SHG, second harmonic generation; THG, third harmonic generation; PERMANOVA, parametric multivariate analysis of variance; ALT, alanine transaminase; AST, aspartate transaminase; FLIM, fluorescence lifetime imaging microscopy.

Bile acids are produced from cholesterol in the liver and metabolized by enzymes encoded by the gut microbiota and are critical for maintaining a healthy gut microbiota (6, 7). Bile acid synthesis is tightly regulated by negative feedback inhibition through the nuclear receptor farnesoid X receptor (FXR) (8). FXR is a transcription factor that binds to the promoter region and initiates the expression of target genes involved in bile acid synthesis and transport and is expressed in the liver, intestine, and kidney. Bile acid compositions of patients with NASH are significantly different from those of healthy subjects (9).

Sevelamer is a nonabsorbable resin used for the treatment of hyperphosphataemia in patients with chronic kidney disease. Substantial protonation of this polymer at physiological pH allows binding and increased fecal excretion of negatively charged phosphate (10). In addition, sevelamer was demonstrated to exert a marked bile acid-binding effect, similar to the second-generation bile acid sequestrant (BAS), colesevelam (11), which is approved as a glucose-lowering drug for the treatment of type 2 diabetes in the United States. Sevelamer was previously demonstrated to elicit significant reductions in plasma glucose concentrations in patients with type 2 diabetes (12).

The potential effects of BAS on reversal of liver injury and prevention of the progression of NASH, however, have not been studied. The current study revealed that treatment with the bile acid sequestrant sevelamer reversed liver injury and prevented the development of NASH, including steatosis, inflammation, and fibrosis in mice with Western diet–induced NAFLD (42% milk fat, 34% sucrose, and 0.2% cholesterol). These results suggest a novel role for BAS treatment in the prevention and treatment of NASH.

Results

Sevelamer intervention decreases the severity of WD-induced NASH

To determine whether sevelamer intervention could decrease the severity of WD-induced NASH, mice were fed a WD for 15 weeks without any treatment and then for an additional 15 weeks either with no treatment or treatment with sevelamer. At the end of the 15-week WD feeding, livers from LF-fed mice showed no steatosis or inflammation, whereas those from WD-fed mice had steatosis, hepatocellular injury, and inflammation. After 15 weeks of sevelamer intervention, there were only small amounts of steatosis, injury, and inflammation (H&E-stained tissue; Fig. 1, *A* and *B*), significant decreases in body weight, liver weight, and fasting serum glucose levels in WD-fed mice (Table 1). These improvements were associated with decreased steatosis and reduced hepatic lipid levels as determined by coherent anti-Stokes Raman scattering (CARS) microscopy imaging (Fig. 1*A*), and liver triglyceride and cholesteryl ester measurements (Fig. 1*C*). Sevelamer intervention also increased fecal cholesterol and triglyceride levels, suggesting an increase in their excretion or a decrease in their absorption (Fig. 1*D*). Importantly, sevelamer intervention decreased the severity of liver fibrosis as determined by Picro Sirius Red (PSR) (Fig. 2, *A* and *B*) and collagen 1 staining (Fig. 2, C and *D*) in WD-fed mice. The reduction in fibrosis was associated with decreases in *Tgfb*, collagen 1a1 (*Col1a1*), and collagen 3a1 (*Col3a1*) mRNA expression (Fig. 2*G*), which indicates that sevelamer treatment may disrupt the pathophysiological processes responsible for collagen deposition. Sevelamer intervention also significantly reduced the pronounced hepatic inflammation found in WD-fed mice, as demonstrated by CD3 immunostaining (Fig. 2, *E* and *F*) and Ccl2 (*Mcp1*) mRNA expression (Fig. 2*G*). Collectively these data show that sevelamer intervention is capable of reversing several of pathological abnormalities that characterize NASH.

Sevelamer prevents WD-induced NASH

NASH is characterized by hepatic steatosis, inflammation, and fibrosis (13). After 24 weeks in the absence of sevelamer, there were marked increases in body, liver, and fat weight in C57BL/6J mice fed the WD (Table 2). In addition, we found that the levels of serum triglycerides, cholesteryl ester, alanine transaminase (ALT), and aspartate transaminase (AST) were significantly elevated in WD-fed mice compared those in LF-fed control mice, which are indicative of impaired liver function and injury (Table 2). H&E-stained sections from livers demonstrated that WD-fed mice exhibited lipid accumulation characterized by a mixture of macro- and microvesicular steatosis (Fig. 3*A*). Label-free imaging with CARS microscopy also revealed increased hepatic neutral lipid accumulation (Fig. 3*A*), which corresponded to marked increases in liver triglyceride and cholesterol contents (Fig. 3*B*). Significantly, the addition of sevelamer to the WD prevented increases in body and liver weight, adipose content, as well as elevation of fasting blood glucose levels and serum triglyceride and cholesterol and ALT and AST levels (Table 2). Additionally, sevelamer administration prevented liver steatosis as determined by H&E staining, CARS microscopy, and biochemical measurement of liver triglyceride and cholesterol content (Fig. 3, *A* and *B*). Moreover, sevelamer treatment prevented the increase in lipid droplet size, as is evident calculated from fluorescence lifetime imaging microscopy (FLIM) images (Fig. 3*C*). The histogram of fat droplets above 85 μm^2 demonstrated that, compared with WD, sevelamer prevented the increase in lipid droplet size to the same size that is seen in LF diet–treated mice (Fig. 3*D*). Importantly, sevelamer prevented the fibrotic changes found in WD-fed mice. Mice fed WD developed significant liver fibrosis, which was ameliorated by sevelamer, as determined by label-free SHG imaging (Fig. 4, *A* and *B*). Sevelamer also prevented profibrotic elevation of *Tgfb*, *Col1a1*, *Col3a1*, and, α-smooth muscle actin (*Acta2*) mRNA expression seen in WD-treated mice (Fig. 4*D*). These results indicate that sevelamer prevents WD-induced fibrosis associated with progressive liver injury.

Sevelamer alters liver lipid profiles in WD-induced NASH

In mouse models of NASH, WD feeding is associated with significant changes in the composition of hepatic lipids linked to disease progression (13, 14). To investigate the effect of sevelamer on WD-induced lipid dysregulation, untargeted lipidomics was carried out on livers from LF-, WD-, and WD plus sevelamer–fed mice. There was clear separation in the principal component analysis (PCA) plots among three groups (Fig. 5*A*). Major ions driving PCA separation were identified based on associated loading scatter plots (Fig. 5*B*). According to the

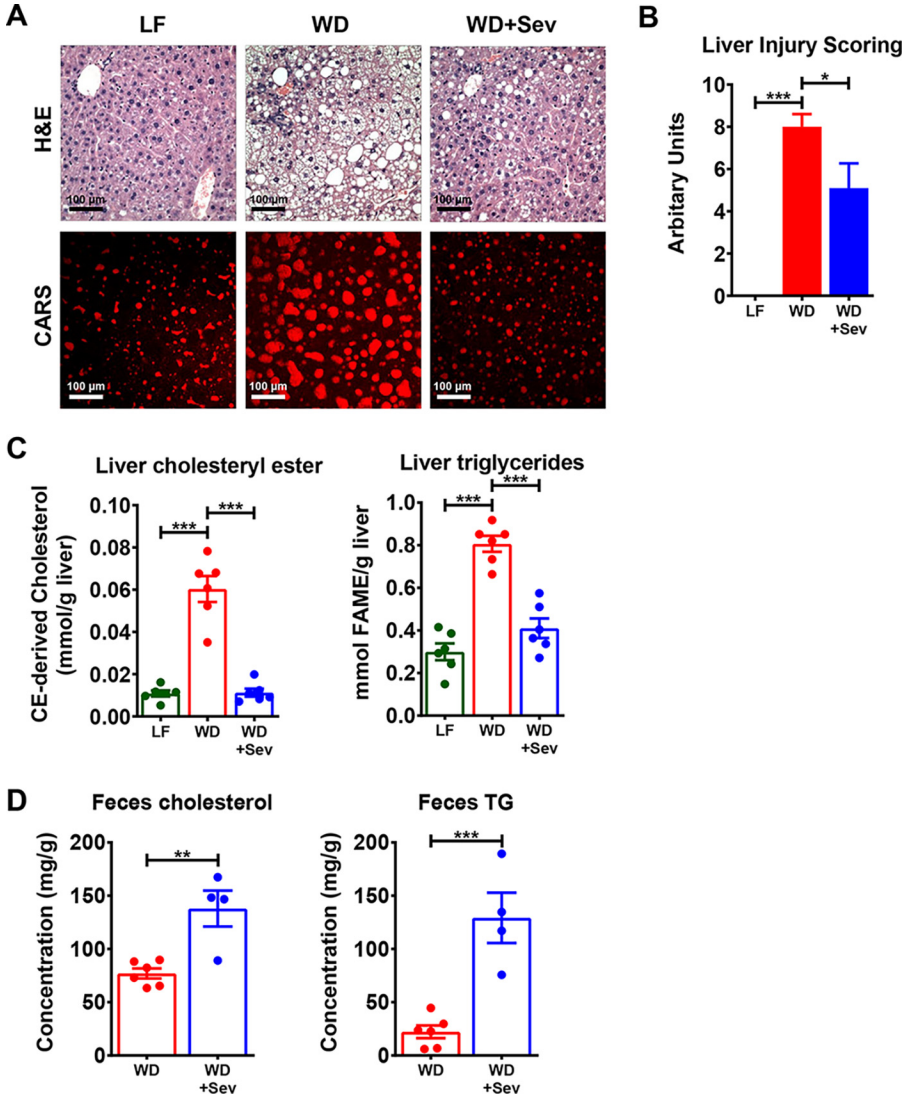

Figure 1. Sevelamer treatment/intervention reverses liver steatosis in WD-induced NASH. *A*, H&E staining and CARS for label-free imaging of lipid deposits in WT mice with LF, WD, or both WD and sevelamer (*Sev*). *B*, liver injury according to the liver injury scoring system. *C*, hepatic triglyceride (*TG*) and cholesteryl ester levels in WT mice fed LW, WD, or WD + sevelamer. *D*, cholesteryl ester and triglyceride excretion in feces ($n = 6$ mice). *, $p < 0.05$; ***, $p < 0.001$.

Table 1
Metabolic parameters for intervention/treatment/reversal studies
The data are means ± S.E. ($n = 6$ mice in each group).

	LF	WD	WD + sevelamer
Body weight (g)	38.4 ± 0.9	49.5 ± 1.1[a]	39.7 ± 1.0[b]
Liver weight (g)	1.58 ± 0.04	3.93 ± 0.22[a]	1.98 ± 0.18[b]
Blood glucose (mg/dl)	218 ± 12.2	233 ± 7.6	187 ± 14.1[b]
Serum ALT (units/liter)	45.3 ± 3.1	88.3 ± 17.2[a]	54.4 ± 13.1[b]
Serum AST (units/liter)	26.5 ± 0.8	48.2 ± 7.2[a]	42.1 ± 3.4

[a] $p < 0.05$ *vs.* LF.
[b] $p < 0.05$ *vs.* WD.

metabolomics database (METLIN MS/MS Database) and MS/MS spectra, these ions were identified, and their relative abundances are depicted in the heat map (Fig. 5*C*). The levels of multiple lipids from different lipid classes, including phosphatidylcholine, phosphoethanolamine, triglyceride, sphingomyelin, cholesterol, lactosylceramide, cholesterol ester, retinol, lysophosphatidylcholine, and diglyceride, were changed by WD feeding. These changes were substantially abrogated by sevelamer treatment. More interestingly, the lipids decreased in WD-treated mice mainly belong to the species with docosahexaenoic acid side chain, whereas they were increased by sevelamer (Fig. 5*C* and Fig. S1).

Sevelamer modifies total bile acid and bile acid composition in WD-induced NASH

Bile acid compositions of patients with NASH are significantly different from those of healthy subjects (9). We measured the levels of individual bile acids in liver, ileum, and cecum (Fig. 6, *A–C*). Total bile acid levels decreased by sevelamer treatment in liver, intestine, and cecum. Moreover, this beneficial effect is associated with changes of bile acid composition (Fig. 6, *A–C*) in LF, WD, and WD + sevelamer–fed mice. The results showed that sevelamer treatment resulted in alterations of individual bile acid species including increased LCA in ileum and decreases in most of the other bile acids (Fig. 6*B*). Bile acids can absorb hydrophobic materials such as cholesterol and phospholipids to form mixed micelles. WD increased the bile acid hydrophobicity index, whereas sevelamer treatment decreased it (Fig. 6*D*). This result indi-

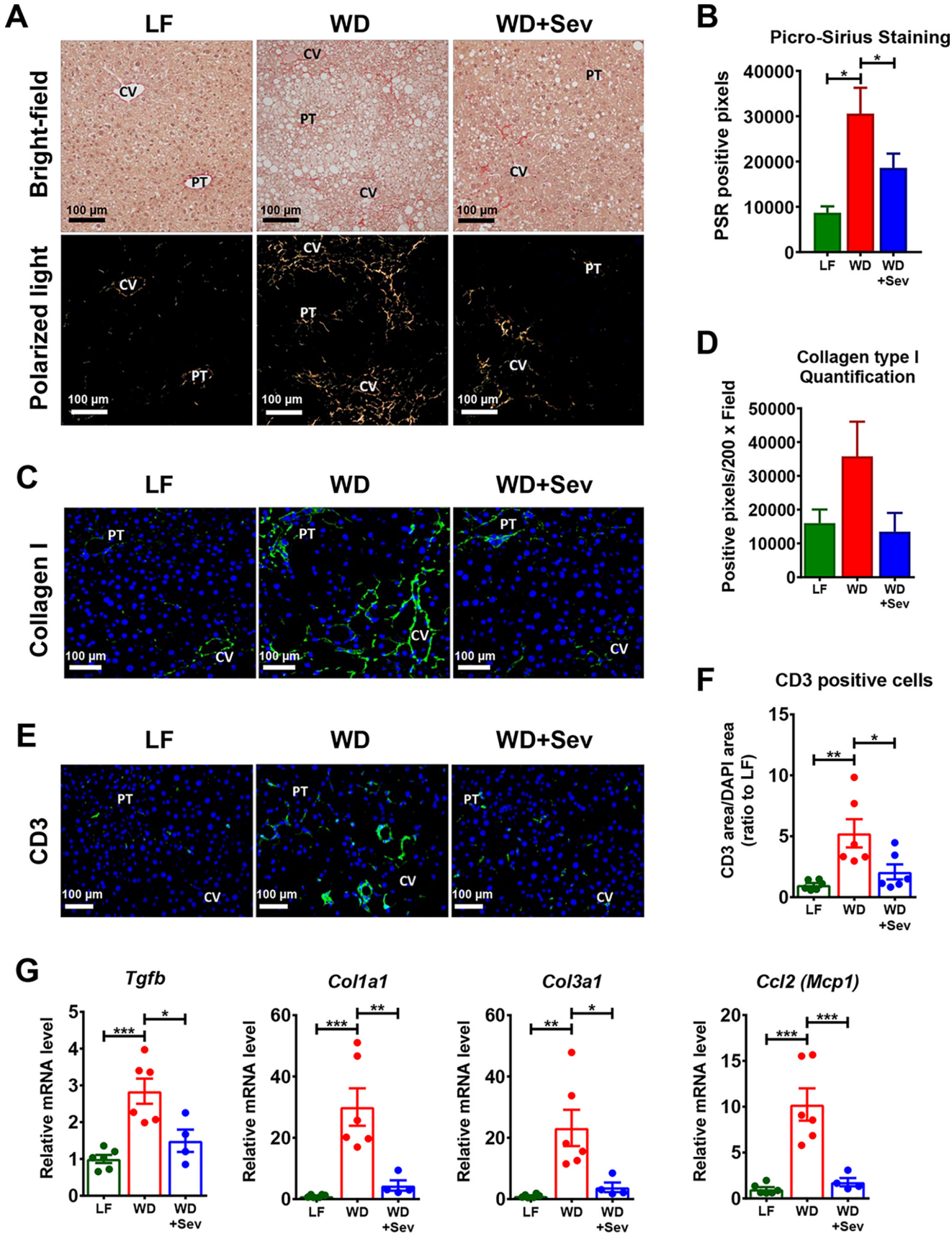

Figure 2. Sevelamer treatment/intervention ameliorates liver fibrosis in WD-induced NASH. *A*, Picro-Sirius Red staining is shown in bright field (*top*) and polarized light (*bottom*). *B*, fibrosis is quantified by PSR staining under polarized light. *C*, collagen I immunostaining. *D*, quantification of collagen I positive. *E*, CD3 immunostaining. *F*, quantification by the ratio of CD3 area to 4′,6′-diamino-2-phenylindole area. *G*, relative mRNA levels of the profibrotic genes transforming growth factor β1 (*Tgfb*), collagen 1a1 (*Col1a1*), and collagen 3a1 (*Col3a1*) in LW, WD, and WD + sevelamer (*Sev*; $n = 4–6$ mice). *, $p < 0.05$. *PT*, portal triad; *CV*, central vein.

Table 2
Metabolic parameters for prevention studies
The data are means ± S.E. ($n = 6$ mice in each group).

	WT LF	WT WD	WT WD + sevelamer
Body weight (g)	36.8 ± 0.3	46.3 ± 2.6[a]	37.9 ± 0.8[b]
Liver weight (g)	1.68 ± 0.06	4.39 ± 0.26[a]	1.69 ± 0.09[b]
Fat weight (g)	7.95 ± 0.31	15.5 ± 1.09[a]	5.64 ± 0.42[b]
Lean weight (g)	24.5 ± 0.35	25.3 ± 0.58	26.9 ± 0.47[b]
Fasting blood glucose (mg/dl)	86.5 ± 7.1	110 ± 7.0[a]	76.3 ± 5.0[b]
Serum ALT (units/liter)	44.9 ± 1.3	78.5 ± 8.0[a]	46.3 ± 0.8[b]
Serum AST (units/liter)	25.4 ± 3.1	39.7 ± 6.1	18.9 ± 1.5[b]
Serum triglycerides (mg/dl)	61.0 ± 12.8	79.4 ± 9.8	34.9 ± 1.8[b]
Serum cholesterol (mg/dl)	138 ± 9.8	252 ± 29.8[a]	139 ± 4.1[b]

[a] $p < 0.05$ *vs.* LF.
[b] $p < 0.05$ *vs.* WD.

cated that sevelamer decreased bile acid hydrophobicity, resulting in decreased lipid absorption from intestine.

Sevelamer modifies WD-induced changes in the gut microbiota

Microbiota of the cecum and colon were profiled in all treatment groups by 16S rRNA gene sequencing. Modest differences (Fig. 7*A*) in overall microbiome composition were noted across all three treatment groups in both the cecum ($p = 0.074$) and colon ($p = 0.12$). Pairwise PERMANOVA tests indicated that these differences were due primarily to the LF *versus* WD comparisons in both cecum ($p = 0.052$) and colon ($p = 0.011$). Furthermore, in the cecum, both LF and WD + sevelamer treatment groups exhibited significantly greater microbial diversity (Shannon's H diversity index) compared with WD ($p = 0.062$ and $p = 0.025$, respectively; Fig. 7*B*); diversity was unchanged across treatment groups in the colon. No differences in microbial richness were noted in either the cecum or colon (Fig. 7*B*). The complex interactions between diet and sevelamer treatment were evident through comparison of the relative abundances of individual taxa between treatment groups (Fig. S2). In all three pairwise comparisons of treatment groups, multiple taxa differed significantly in relative abundance. Of note, the genus *Lactobacillus* (phylum Firmicutes) was depleted in the WD group compared with both LF and WD + sevelamer ($p < 0.05$ and $p < 0.01$, respectively). In contrast, the proteobacterial genus *Desulfovibrio* was enriched in WD compared with both LF and WD + sevelamer ($p < 0.05$ for each comparison). However, many other taxa differed between LF and WD + sevelamer animals, indicating that sevelamer treatment did not simply reverse the shifts of colonic microbiota observed in WD animals (*i.e.* LF *versus* WD).

As described above, bile acid pools were altered by both WD and sevelamer treatment. Because intestinal bile acids not only act as anti-microbial agents but are metabolized by selected gut microbes (15), we hypothesized that shifts in bile acid pools in the intestinal lumen might underlie the observed changes in gut microbiota. Consequently, concentrations of cecal bile acid species of LF, WD, and WD + sevelamer mice were correlated with the relative abundances of cecal and colon microbiota (Fig. 7*C*). In both anatomical sites, selected bacterial taxa were significantly associated (either positively or negatively) with a range of bile acid species. However, hierarchical clustering did not segregate bile acid species by taurine conjugation status or bacterial genera by phylum-level affiliation. For example, the genera *Lactobacillus* (of the phylum Firmicutes) and *Alistipes* (of the phylum Bacteroidetes) were negatively correlated with several conjugated and unconjugated bile acids, whereas diverse Firmicutes (*Anaerotruncus*, *Coprococcus*, *Turicibacter*, and *Lachnospiraceae*) were positively correlated with the same bile acid species.

Discussion

The present study indicates that bile acid sequestration sevelamer prevents and treats WD-induced NASH in mice, by decreasing the NASH hallmarks of lipid accumulation, inflammation, and fibrosis. Moreover, sevelamer was found to modulate the gut microbiome and bile acid metabolism, resulting in reversing microbiome complexity in cecum and increasing *Lactobacillus* and decreased inflammation related bacteria *Desulfovibrio*. Recent evidence indicates that treatment strategies for improving bile acid metabolism may prevent or slow the progression of liver disease (16–18). Bile acid sequestrants are orally administered nonabsorbable polymers that bind bile acids in the intestine to form nonabsorbable complexes, interrupting the enterohepatic circulation of intestinal bile acids. The present studies show that BAS treatment prevents and decreases the severity of manifestations of WD-induced (42% milk fat, 34% sucrose, and 0.2% cholesterol) NASH in C57BL/6J mice, including the decreases in serum AST, ALT, and lipids (Fig. 1 and Table 1) as determined by CARS for label-free imaging of lipid deposits (19–21). Fibrosis is characterized by the excessive accumulation of extracellular matrix components, leading to disrupted tissue function in affected organs. Progressive fibrosis is the hallmark of NASH disease progression, and therefore, reducing fibrosis is an important goal of therapy. Sevelamer treatment prevents fibrosis in the liver on WD-induced NASH model, whereas mice fed WD developed significant liver fibrosis, which is associated with significant increases in liver profibrotic genes. These results indicated that sevelamer/bile acid sequestration might be possible candidates for treatment of human NASH.

The human gut microbiota includes 10–100 trillion microorganisms, mainly bacteria, that vastly outnumber our own human cells (22). The term dysbiosis refers to disruption of the normal gut microbiota. Dysbiosis has been described in patients with obesity (23) or other features of metabolic syndrome (24), established NASH (25–27), and T2DM (28–31). Several studies have stressed the role of the gut microbiota in NASH (26, 32–34), but causality is yet to be established. Patients with NASH have a higher prevalence of small intestinal bacterial overgrowth (35, 36) and microbial dysbiosis (26). A potential role for sevelamer in modifying the gut microbiome was identified. In the cecum, both sevelamer treatment of WD-fed mice reversed microbial diversity similar to the LF-fed groups. Notably, the genus *Lactobacillus* (phylum Firmicutes) was depleted in the WD group compared with both LF and WD + sevelamer. In contrast, the proteobacterial genus *Desulfovibrio* was enriched in WD compared with both LF and WD + sevelamer. *Desulfovibrio* are consistently associated with the development of obesity, adipose tissue, and systemic inflammation and metabolic comorbidities in both humans (29,

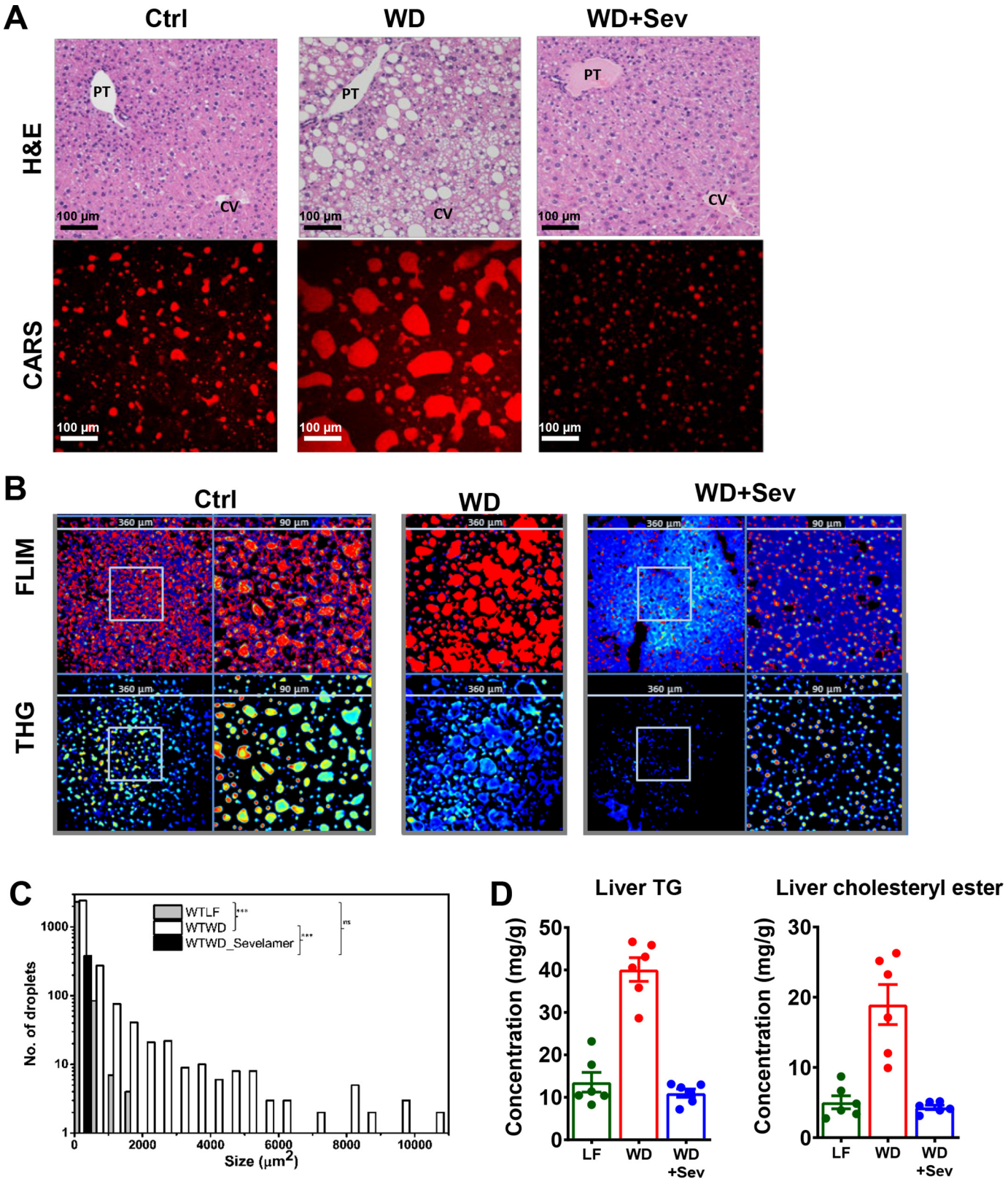

Figure 3. Treatment of WD-fed mice with sevelamer prevents liver steatosis. *A*, sevelamer administration prevents liver steatosis in both WD-induced WT mice as determined by H&E staining and CARS microscopy. *B*, intensity (*top*), FLIM (mapped for fat droplets in *red areas*) (*middle*), and THG (*bottom*) images of samples from LF, WD, and WD + sevelamer (*Sev*). The control and WD + sevelamer images have two panels. The *left panel* is 360 μm, and the *right one* is zoomed in at 90 μm, which is the central part of the *left panel*. THG and FLIM shows that the same droplets are imaged using FLIM and THG. *C*, the histogram of the size of fat droplets was calculated based on the *red areas* in the FLIM images. *D*, hepatic triglyceride (*TG*) and cholesteryl ester levels ($n = 6$ mice). *, $p < 0.05$; ***, $p < 0.001$. *Ctrl*, control. *PT*, portal triad; *CV*, central vein.

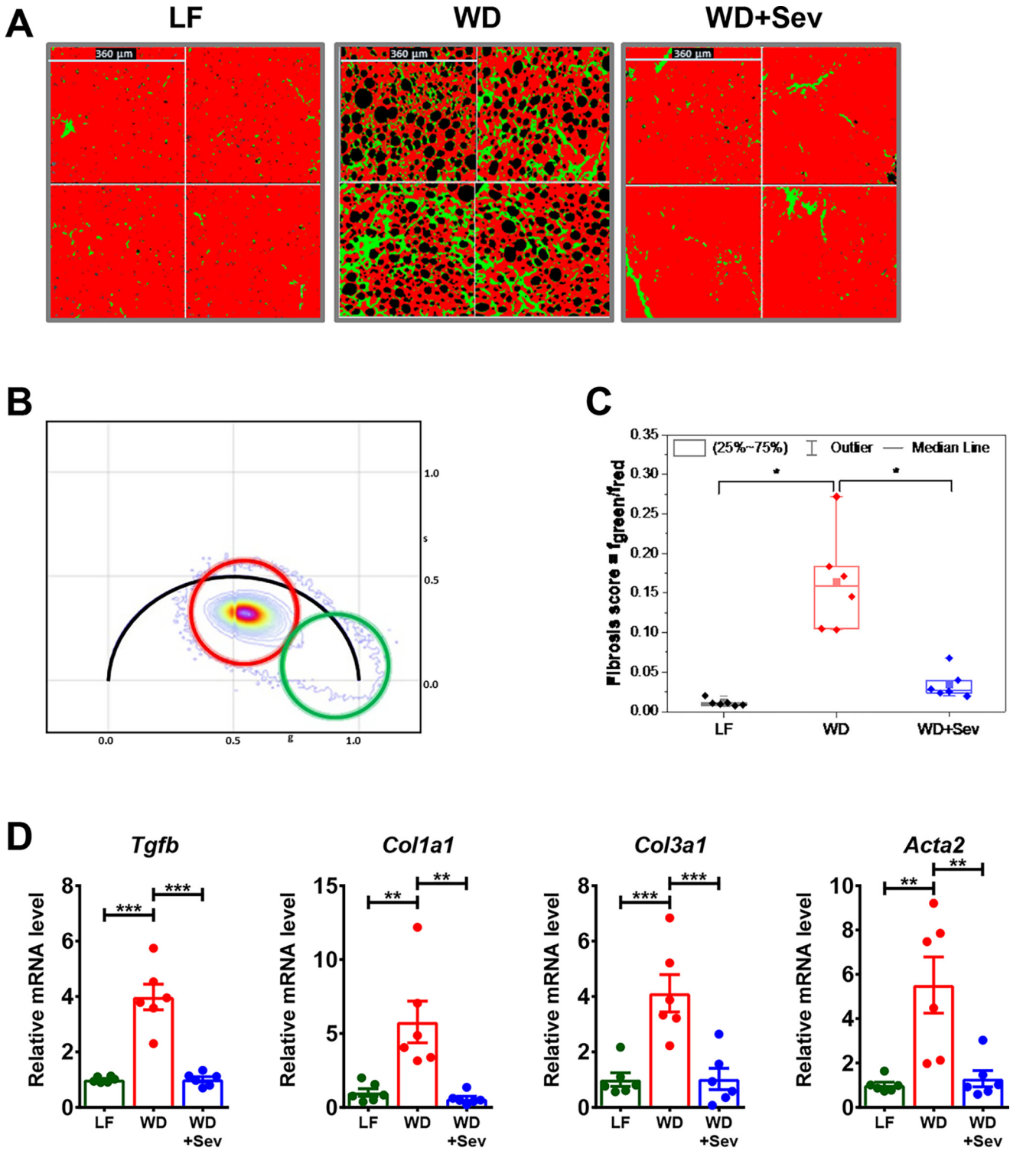

Figure 4. Treatment of WD-fed mice with sevelamer prevents fibrosis. *A*, representative SHG images of liver tissues obtained using the Diver microscope with LF, WD, and WD + sevelamer (*Sev*). *Green* signal represents SHG from collagen. *Red color* represents autofluorescence from rest of the tissue. *B*, collagen SHG was selected using the *green cursor* of the phasor map, and the *red cursor* was used to map the autofluorescence. *C*, quantification of SHG signal by *green/red* ratio. *D*, mRNA expressions of profibrotic genes *Tgfb*, *Col1a1*, *Col3a1*, and *Acta2* in liver of mice fed LF, WD, and WD + sevelamer ($n = 6$ mice). *, $p < 0.05$; **, $p < 0.01$; ***, $p < 0.001$.

37) and rodents (38). These studies further document that the anti-inflammatory effects are also associated with the prevention and decreased severity of liver fibrosis.

A recent study revealed that the intestine-restricted FXR agonist fexaramine markedly increased taurolithocholic acid, increased secretion of GLP-1, and improved insulin and glucose tolerance by TGR5 activation (39). Fexaramine treatment increased the abundance of *Helicobacter*, *Alistipes*, *Bacteroides*, *Anaeroplasma*, *Flavonifractor*, *Acetatifactor*, and *Shewanella*. In the present study, *Alistipes* were correlated with LCA and

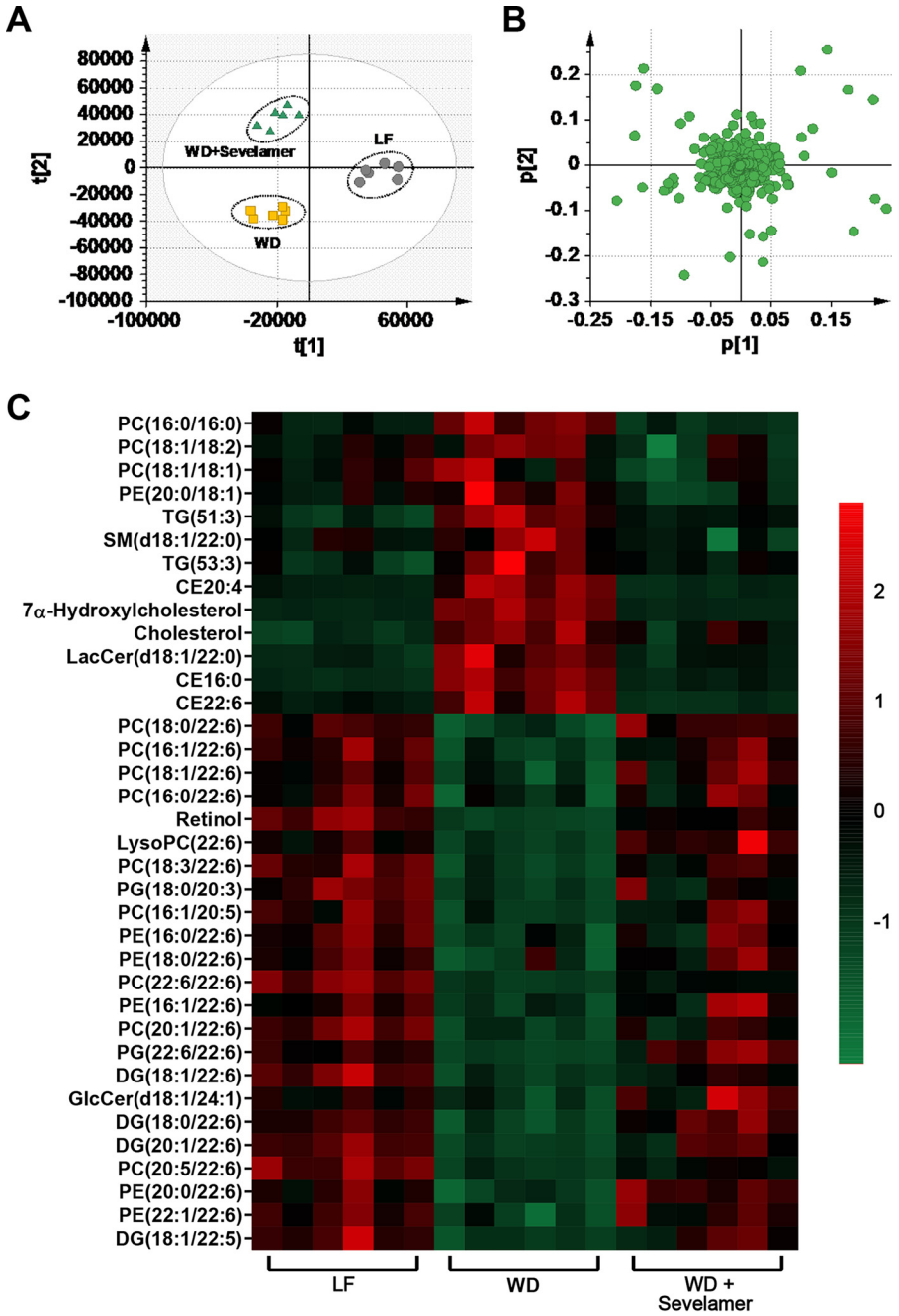

Figure 5. Western diet and sevelamer modulate lipid metabolism in liver. *A*, PCA. *B*, score scatter plots of the liver lipid metabolites from LF, WD, and WD + sevelamer (6 mice/group). *t[1]* and *t[2]* correspond to principal components 1 and 2, respectively. The *p[1]* values represent the interclass difference, and *p[2]* values represent the relative abundance of the ions. The data were obtained in positive mode (ESI +). *C*, heat map of lipid metabolites in liver of LF, WD, and WD + sevelamer–treated mice (6 mice/group). *CE*, cholesteryl ester; *DG*, diacylglycerol; *PC*, phosphatidylcholine; *PE*, phosphatidylethanolamine; *PG*, phosphatidylglycerol; *SM*, sphingomyelin; *TG*, triacylglycerol.

taurolithocholic acid levels in colon. Traditionally, the functions of bile acids are thought to stimulate hepatic bile flow and to aid in the digestion and absorption of fats from the intestinal lumen (40). Sevelamer treatment altered individual bile acid species, increased LCA in ileum, and decreased most of the other bile acids. However, *Gcg* mRNA levels were not changed following treatment with sevelamer, suggesting that TGR5-GLP1 might not be related to attenuation of the mouse NASH by sevelamer treatment in this study (Fig. S3). On the other hand, *Fgf15* and *Shp* mRNA expression increased in WD-treated group, whereas *Fxr*, *Fgf15*, and *Shp* mRNA expression decreased in the WD + sevelamer group. It was shown that FXR inhibition in intestine decreases NASH in mice, and BAS reverses innate immune dysregulation in NAFLD model mice (41, 42). A novel finding of the present study was the effects of long-term bile acid sequestration by sevelamer in preventing steatosis, inflammation, and fibrosis, associated with modulation of *Fxr*, *Fgf15*, and *Shp* expression (Fig. S3).

Together with host genotype and lifestyle (energy intake and expenditure), the gut microbiota contributes significantly to

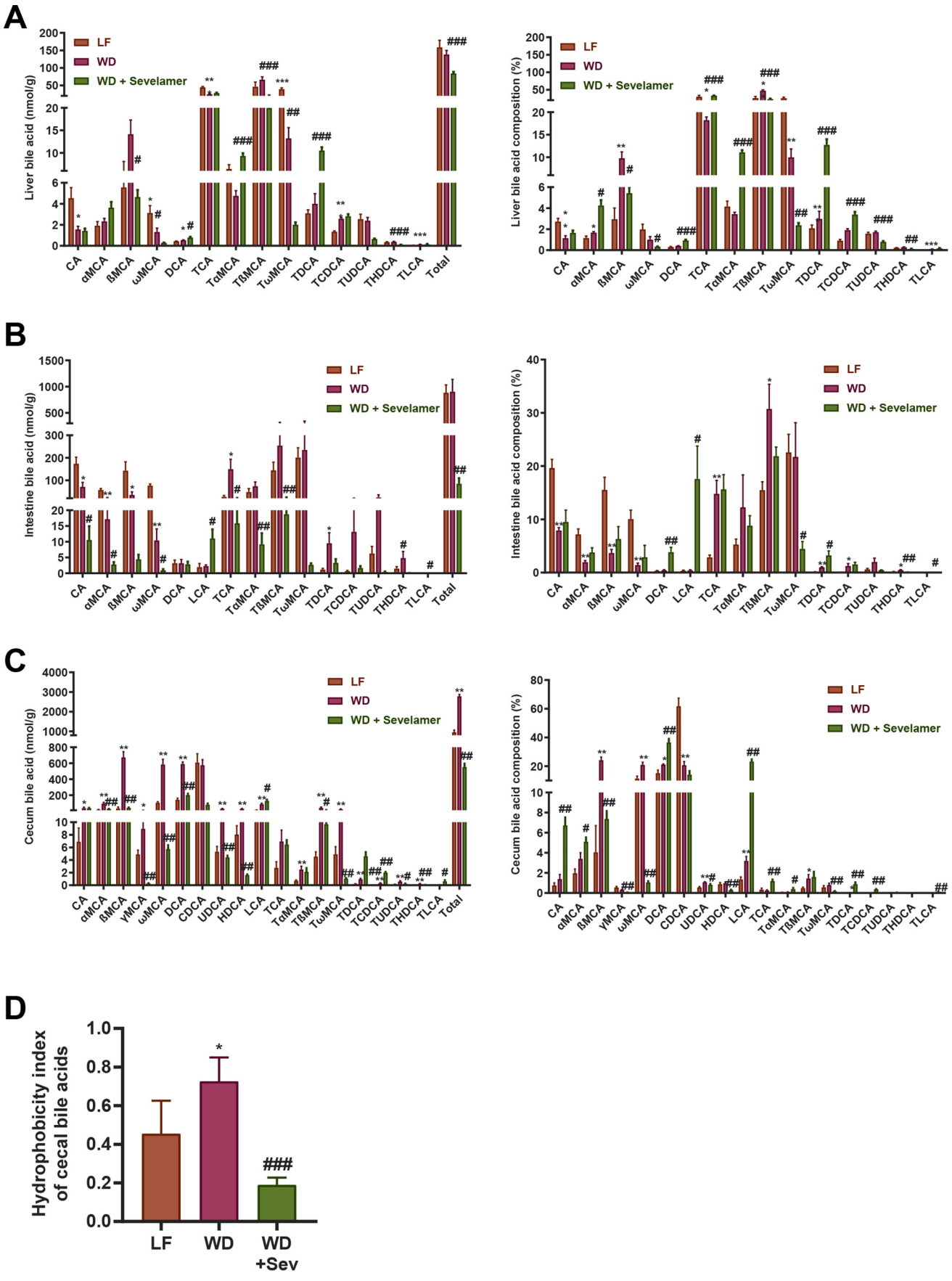
A
Liver bile acid (nmol/g)
Liver bile acid composition (%)
B
Intestine bile acid (nmol/g)
Intestine bile acid composition (%)
C
Cecum bile acid (nmol/g)
Cecum bile acid composition (%)
LF
WD
WD + Sevelamer
CA
αMCA
βMCA
ωMCA
DCA
LCA
TCA
TαMCA
TβMCA
TωMCA
TDCA
TCDCA
TUDCA
THDCA
TLCA
Total
γMCA
CDCA
UDCA
HDCA
D
Hydrophobicity index of cecal bile acids
WD +Sev

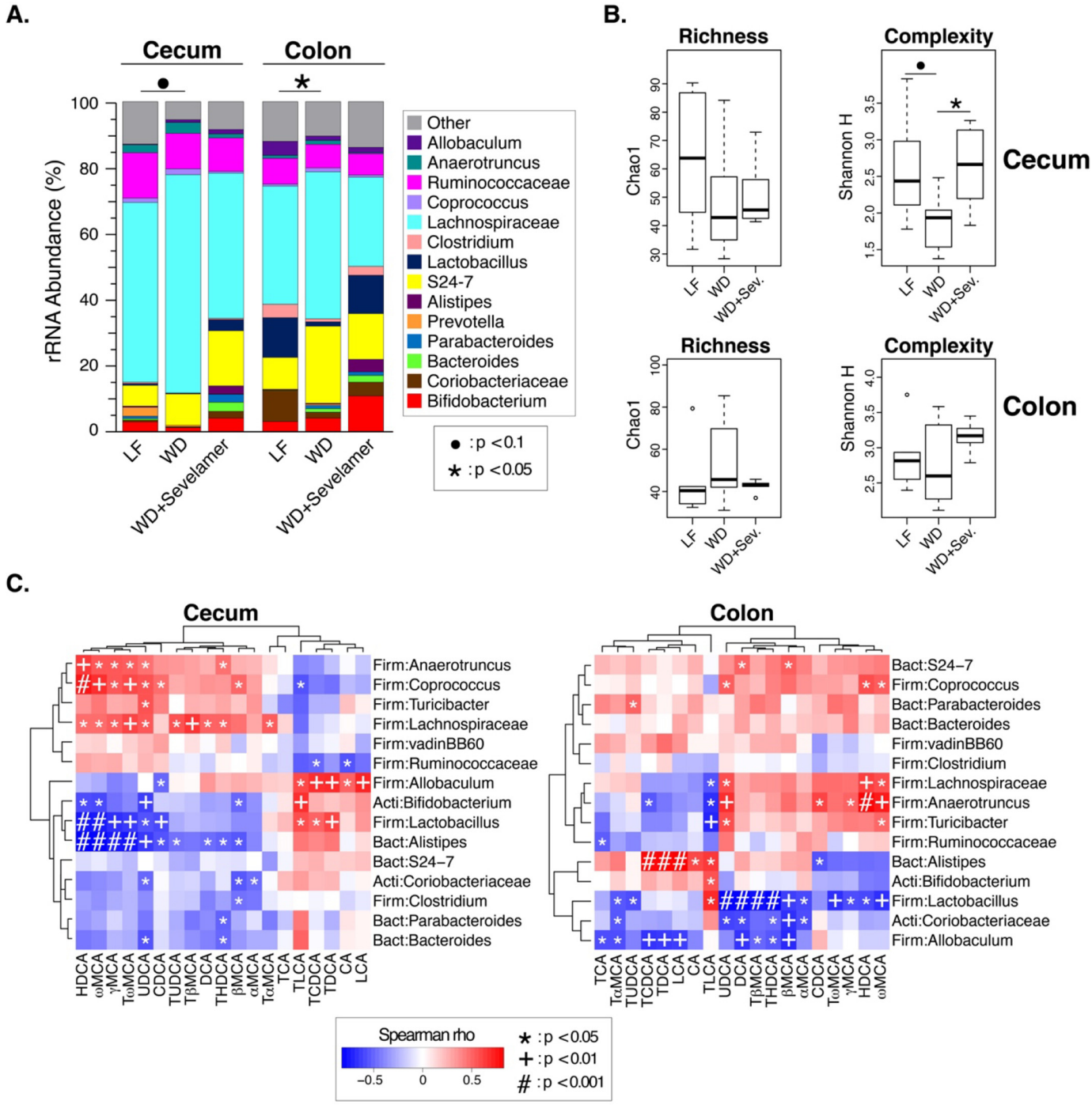

Figure 7. WD and sevelamer modulate the microbiota. *A*, distribution of bacterial genera in cecal and colon contents. The results of PERMANOVA tests for pairwise comparisons between treatment groups are shown by *symbols* above bar charts. *B*, summary of biodiversity indices estimating ecological richness (Chao1) and complexity (Shannon H) across groups in the cecum and colon. ●, $p < 0.1$; *, $p < 0.05$. *C*, heat maps displaying Spearman Rho correlation coefficients for pairwise comparisons of cecal bile acid species *versus* cecal or colonic microbial taxa (top 15 most abundant genus-level taxa). *, $p < 0.05$; +, $p < 0.01$; #, $p < 0.001$. Taxon names are preceded by abbreviated phylum names: *Acti*, Actinobacteria; *Bact*, Bacteroidetes; *Firm*, Firmicutes.

Figure 6. Western diet and sevelamer modulate bile acid levels in liver, ileum, and cecum. *A*, individual and total bile acid levels and composition of liver of WT mice with control diet, WD, or both WD and sevelamer (*Sev*). *B*, individual and total bile acid levels of ileum of LF-, WD-, and WD + sevelamer–fed mice. *C*, individual and total bile acid levels of cecum of LF-, WD-, and WD + sevelamer–fed mice. *D*, hydrophobicity index of cecal bile acids in LF-, WD-, and WD + sevelamer–fed mice. $n = 6$ mice. * indicates statistically difference between LF and WD. # indicates statistically difference between WD and WD + Sev. *, #, $p < 0.05$; **, ##, $p < 0.01$; ***, ###, $p < 0.001$. *CA*, cholic acid; *CDCA*, chenodeoxycholic acid; *UDCA*, ursodeoxycholic acid; *HDCA*, hyodeoxycholic acid; *DCA*, deoxycholic acid; *αMCA*, α-muricholic acid; *βMCA*, β-muricholic acid; *ωMCA*, ω-muricholic acid; *T*-, tauro-.

the pathophysiology of metabolic disease through modulation of both energy harvest and enteroendocrine signaling (25, 43–45). Both bile acid pool size and composition are important factors in regulating gut microbial community structure (46, 47). Thus, sevelamer may mediate its effects on host metabolism in part through alteration of gut microbiome function. It should be noted that the changes in microbiota reported herein are largely descriptive. Future studies, for instance, using microbial transplants into germ-free mice will aid in the delineation of the functional consequences to host metabolism of sevelamer-induced changes in gut microbiota.

In addition to using classical histological techniques, the present work also applied novel label-free imaging techniques, including CARS and THG microscopy for quantitative detection of steatosis and lipid droplet size and FLIM-SHG for quantitative detection of fibrosis. In future studies, we will consider applying the DIVER microscope for *in situ* imaging of the liver in mouse models of NASH and their response to additional treatment modalities.

Experimental procedures

Animal models

All animal experiments and protocols were approved by the Animal Care and Use Committees at the University of Colorado, Anschutz Medical Campus and Georgetown University. Animal experimentation was conducted in accordance with the Guide for Care and Use of Laboratory Animals of the National Institutes of Health (Bethesda, MD).

Prevention study

Six-week-old male C57BL/6J mice were purchased from Jackson Laboratories (Bar Harbor, ME). After 1 week of acclimation they were fed a Harlan Teklad TD.88137 Western diet of 42% milk fat, 34% sucrose, and 0.2% cholesterol with or without sevelamer carbonate 2% (2 g/100 g of diet) or a matched 10% fat, Harlan Teklad TD.08485 LF diet for 24 weeks. The mice were killed, and blood, liver, and intestinal contents were harvested at the end of the 24-week treatment period.

Intervention study

After a week of acclimation, 6-week-old male C57BL/6J mice were fed a LF diet or WD for 15 weeks. After the 15-week diet treatment, the mice were further fed for another 15 weeks without or with sevelamer carbonate 2% (2 g/100 g of diet) added to the diets. The mice were killed at the end of the 30-week treatment period, and blood and organs were collected.

Determination of fat weight

Body composition was performed noninvasively by quantitative magnetic resonance (EchoMRI-900 whole-body composition analyzer; Echo Medical Systems, Houston, TX).

Blood chemistry

Blood glucose levels were measured with a Glucometer Elite XL (Bayer, Tarrytown, NY). Cholesterol (Wako Chemicals, Richmond, VA), triglycerides (Wako Chemicals, Richmond, VA), ALT (Bioassay Systems, Hayward, CA), and AST (Bioassay Systems, Hayward, CA) were measured according to the manufacturers' instructions.

Measurement of stool triglyceride and cholesterol content

Forty-eight hours after the initiation of treatment with sevelamer, WD or WD + sevelamer mice were placed in metabolic balance cages for a 72-h collection of stool while they were fed *ad libitum* water and diets. The lipids were extracted from stool based on a method reported earlier (48) and analyzed for cholesterol and triglycerides (Wako Chemicals, Richmond, VA).

RNA extraction and real-time quantitative PCR

Total RNA was isolated from the livers using Qiagen RNeasy mini kit, and cDNA was synthesized using reverse transcript reagents from Bio-Rad. Quantitative real-time PCR was performed as previously described (49, 50). The primer sequences are listed in Table S1.

Histological stains

After formalin fixation, tissues were processed and embedded into paraffin. 5-μm-thick sections were cut onto glass slides. Following H&E staining, the liver sections were scored per the liver scoring system described by Lanaspa *et al.* (51). Histological images of H&E-stained tissue were captured on an Olympus BX51 microscope equipped with a four-megapixel Macrofire digital camera (Optronics, Goleta, CA). All images were cropped and assembled using Photoshop CS2 (Adobe Systems, Inc., Mountain View, CA). For PSR staining, the slides were first immersed in Bouin's fixative for 30 min. Then the hydrated slides were immersed in Sirius Red solution (Direct Red 80 and saturated picric acid, Sigma) and briefly washed with 0.5% acetic acid (Thermo Fisher Scientific, Waltham, MA). Slides stained with either H&E or PSR were mounted using Cytoseal XYL, a xylene-based mounting medium (Richard-Allen Scientific, Kalamazoo, MI). For quantification of the fibrosis following PSR staining, nine 100× polarized light images were made in a "tiling" fashion across each PSR stained slide and then quantified using the 3I Slidebook program (3I, Denver, Colorado) to arrive at the PSR-stained pixels per 100× field for that slide. The liver injury was scored according to a method described earlier in detail (19, 51), and the scoring was blindly performed.

Immunohistochemistry

The tissues were stained immunohistochemically for collagen type 1 (600-401-D19; Rockland, Limerick, PA) as previously described (20). Immunoreactivity was visualized with secondary antibodies conjugated to Alexa Fluor 488 or Alexa Fluor 594 at dilutions of 1:500 and 1:250, respectively. Nuclei were stained with 4′,6-diamidino-2-phenylindole (Sigma–Aldrich). Immunofluorescence images were captured on a Nikon Diaphot fluorescence microscope and digitally deconvolved using the No Neighbors algorithm (Slidebook, Denver, CO) as previously described (20). All images were cropped and assembled using Photoshop CS2 (Adobe Systems, Inc.). For quantification of the immunofluorescence, eight 100× polarized light images were made, each encompassing a portal triad to central vein

field, and then quantified using the 3I Slidebook program (3I) to arrive at the immunofluorescent positively stained pixels per 200× field. To compare multiple experiments, the data were expressed as a ratio to the low fat–treated group.

Measurement of hepatic triglyceride and cholesterol contents

Triglycerides and cholesterol esters were measured with GC-MS, as detailed in the supporting text (14).

Serum and tissue bile acid composition analysis

Bile acid composition was determined by an Acquity® UPLC/G2Si QTOFMS system (Waters Corp.) with an electrospray ionization (ESI) source. An Acquity® BEH C18 column (100 × 2.1 mm; internal diameter, 1.7 mm; Waters Corp.) was applied for chromatographic separation. A mixture of 0.1% formic acid in water (A) and 0.1% formic acid in acetonitrile (B) was used as the mobile phase. The gradient elution was started from 80% A for 4 min, decreased linearly to 60% A over 11 min, to 40% A over the next 5 min, to 10% A for the succeeding 1 min, and finally increased to 80% A for 4 min to re-equilibrate the column. Column temperature was maintained at 45 °C, and the flow rate was 0.4 ml/min. Mass spectrometry detection was operated in negative mode. A mass range of m/z 50–1200 was acquired (53).

Lipidomics analysis

For lipidomics, about 70 mg of liver tissue was accurately weighed and homogenized with 700 μl of methanol:H_2O (4:3, v/v) solution and then extracted using 800 μl of chloroform containing sphingomyelin (17:0), phosphatidylcholine (17:0), and ceramide (17:0) at 1 μM as internal standards. The homogenate was shaken and incubated at 37 °C for 20 min followed by centrifugation at 15,000 × g for another 15 min. The lower organic phase was collected and evaporated to dryness under vacuum. The residue was then suspended with 100 μl of chloroform:methanol (1:1, v/v) solution and then diluted with isopropanol:acetonitrile:H_2O (2:1:1, v/v/v) solution before injection. Lipidomics analysis was performed on an Acquity® UPLC/G2Si QTOFMS system (Waters Corp., Milford, MA) equipped with an ESI source. Separation was achieved on an Acquity® UPLC CSH C18 column (100 × 2.1 mm; internal diameter, 1.7 mm; Waters Corp.). The mobile phase was a mixture of acetonitrile/water (60/40, v/v, A) and isopropanol/acetonitrile (90/10, v/v, B), and both A and B contained 10 mM ammonium acetate and 0.1% formic acid. The gradient elution program consisted of a 2-min linear gradient of 60% A to 57% A, to 50% A at 2.1 min*, a linear decrease to 46% A at 12 min, to 30% A at 12.1 min*, a linear decrease to 1% A at 18 min before returning to initial conditions at 18.5 min to equilibrate the column (*indicates ballistic gradient). The column temperature was maintained at 55 °C, and the flow rate was 0.4 ml/min. Mass spectrometry data were acquired in the both positive and negative ESI modes at a range of m/z 100–1,200 (41).

CARS microscopy

CARS microscopy was performed for label-free imaging of lipid deposits as previously described (54–57) and as detailed in the supporting text.

Autofluorescence FLIM, SHG, and THG measurements using DIVER microscope

To determine the effects of WD and treatment with sevelamer on lipids and fibrillary collagens, autofluorescence FLIM, SHG, and THG signals were acquired using the DIVER (deep imaging via enhanced-photon recovery) microscope developed at the Laboratory of Fluorescence Dynamics, University of California at Irvine, as detailed in the supporting text.

Microbiome analysis

Bacterial profiles were determined by broad-range analysis of 16S rRNA genes following a previously described method (58–60). DNA was extracted from 50–100 mg of cecal or colon contents using the QIAmp stool DNA isolation kit (Qiagen). Broad-range PCR amplicons were generated using barcoded primers (61) targeting the 16S rRNA gene V3V4 variable region: primers 338F (5′-ACTCCTACGGGAGGCAGCAG) and 806R (5′ GGACTACHVGGGTWTCTAAT) (62, 63). Illumina paired-end sequencing was performed on the MiSeq platform using a 600-cycle version 3 reagent kit. Demultiplexed paired-end reads were assembled using phrap (64), and pairs that did not assemble were discarded. Assembled sequence ends were trimmed over a moving window of five nucleotides until average quality met or exceeded 20. Trimmed sequences with more than 1 ambiguity or shorter than 150 nucleotides were discarded. Potential chimeras identified with Uchime (usearch6.0.203_i86linux32) (65) using the Schloss (66) Silva reference sequences were removed from subsequent analyses. Assembled sequences were aligned and classified with SINA (1.3.0-r23838) (67) using the bacterial sequences in Silva 115NR99 (68) as reference configured to yield the Silva taxonomy. Operational taxonomic units were produced by clustering sequences with identical taxonomic assignments.

Statistical analysis

The results are presented as the means ± S.E., and the data were analyzed by analysis of variance and Student–Newman–Keuls tests for multiple comparisons or by t test for unpaired data between two groups (GraphPad Prism). Ratiometric SHG and histogram of steatosis by autofluorescence images were analyzed using a two-sample t test for variance and a Kolmogorov–Smirnov test for histograms (Origin; OriginLab Corp, Northampton, MA), respectively. Statistical significance was accepted at the $p < 0.05$ level, and *** was added for $p < 0.005$.

Microbiome analyses used Explicet (69) and the R statistical software package (52). The relative abundance of each taxon was calculated as the number of 16S rRNA sequences of a given taxon divided by the total number of 16S rRNA sequences in a patient's sample. Differences in overall microbiome composition (*i.e.* β-diversity) between subsets were assessed by a PERMANOVA test using Morisita–Horn dissimilarities; p values were estimated through 1,000,000 permutations. Shannon diversity, Shannon evenness, and richness (species-observed) were calculated using rarefaction and compared across groups through analysis of variance tests. Comparisons of relative abundance across groups were conducted by nonparametric Kruskal–Wallis tests. Associations between cecal bile acid spe-

cies concentrations and relative abundances of genus-level bacterial taxa were assessed by Spearman rank-sum correlation tests.

Author contributions—S. T., Y. L., S. R., C. X., D. J. O., X. X. W., D. I., D. N. F., and M. L. investigation; S. T., Y. L., C. X., and D. N. F. writing-original draft; S. R., A.E.L., D. J. O., A. D., K. W. K., E. G., D. N. F., and M. L. methodology; D. J. O., X. X. W., K. M., B. A. J., K. B., D. W., J. L. M., E. G., C. E. R., F. J. G., and M. L. writing-review and editing; M. L. conceptualization; M. L. resources; M. L. formal analysis; M. L. supervision; M. L. funding acquisition; M. L. project administration.

References

1. Arab, J. P., Karpen, S. J., Dawson, P. A., Arrese, M., and Trauner, M. (2017) Bile acids and nonalcoholic fatty liver disease: molecular insights and therapeutic perspectives. *Hepatology* **65,** 350–362 CrossRef Medline
2. Hendrikx, T., Watzenböck, M. L., Walenbergh, S. M., Amir, S., Gruber, S., Kozma, M. O., Grabsch, H. I., Koek, G. H., Pierik, M. J., Staufer, K., Trauner, M., Kalhan, S. C., Jonkers, D., Hofker, M. H., Binder, C. J., *et al.* (2016) Low levels of igm antibodies recognizing oxidation-specific epitopes are associated with human non-alcoholic fatty liver disease. *BMC Med.* **14,** 107 CrossRef Medline
3. Leung, C., Rivera, L., Furness, J. B., and Angus, P. W. (2016) The role of the gut microbiota in NAFLD. *Nat. Rev. Gastroenterol. Hepatol.* **13,** 412–425 CrossRef Medline
4. Betrapally, N. S., Gillevet, P. M., and Bajaj, J. S. (2016) Changes in the intestinal microbiome and alcoholic and nonalcoholic liver diseases: causes or effects? *Gastroenterology* **150,** 1745–1755.e3 CrossRef Medline
5. Loomba, R., Seguritan, V., Li, W., Long, T., Klitgord, N., Bhatt, A., Dulai, P. S., Caussy, C., Bettencourt, R., Highlander, S. K., Jones, M. B., Sirlin, C. B., Schnabl, B., Brinkac, L., Schork, N., *et al.* (2017) Gut microbiome based metagenomic signature for non-invasive detection of advanced fibrosis in human nonalcoholic fatty liver disease. *Cell Metab.* **25,** 1054–1062.e5 CrossRef Medline
6. Wahlström, A., Sayin, S. I., Marschall, H.-U., and Bäckhed, F. (2016) Intestinal crosstalk between bile acids and microbiota and its impact on host metabolism. *Cell Metab.* **24,** 41–50 CrossRef Medline
7. Tripathi, A., Debelius, J., Brenner, D. A., Karin, M., Loomba, R., Schnabl, B., and Knight, R. (2018) The gut–liver axis and the intersection with the microbiome. *Nat. Rev. Gastroenterol. Hepatol.* **15,** 397–411 CrossRef Medline
8. Sinal, C. J., Tohkin, M., Miyata, M., Ward, J. M., Lambert, G., and Gonzalez, F. J. (2000) Targeted disruption of the nuclear receptor fxr/bar impairs bile acid and lipid homeostasis. *Cell* **102,** 731–744 CrossRef Medline
9. Ferslew, B. C., Xie, G., Johnston, C. K., Su, M., Stewart, P. W., Jia, W., Brouwer, K. L., and Barritt, A. S., 4th (2015) Altered bile acid metabolome in patients with nonalcoholic steatohepatitis. *Dig. Dis. Sci.* **60,** 3318–3328 CrossRef Medline
10. Brønden, A., Hansen, M., Sonne, D. P., Rohde, U., Vilsbøll, T., and Knop, F. K. (2015) Sevelamer in a diabetologist's perspective: a phosphate-binding resin with glucose-lowering potential. *Diabetes Obes. Metab.* **17,** 116–120 CrossRef Medline
11. Braunlin, W., Zhorov, E., Guo, A., Apruzzese, W., Xu, Q., Hook, P., Smisek, D. L., Mandeville, W. H., and Holmes-Farley, S. R. (2002) Bile acid binding to sevelamer HCl. *Kidney Int.* **62,** 611–619 CrossRef Medline
12. Vlassara, H., Uribarri, J., Cai, W., Goodman, S., Pyzik, R., Post, J., Grosjean, F., Woodward, M., and Striker, G. E. (2012) Effects of sevelamer on hba1c, inflammation, and advanced glycation end products in diabetic kidney disease. *Clin. J. Am. Soc. Nephrol.* **7,** 934–942 CrossRef Medline
13. Orlicky, D. J., Libby, A. E., Bales, E. S., McMahan, R. H., Monks, J., La Rosa, F. G., and McManaman, J. L. (2019) Perilipin-2 promotes obesity and progressive fatty liver disease in mice through mechanistically distinct hepatocyte and extra-hepatocyte actions. *J. Physiol.* **597,** 1565–1584 CrossRef Medline
14. Libby, A. E., Bales, E., Orlicky, D. J., and McManaman, J. L. (2016) Perilipin-2 deletion impairs hepatic lipid accumulation by interfering with sterol regulatory element-binding protein (SREBP) activation and altering the hepatic lipidome. *J. Biol. Chem.* **291,** 24231–24246 CrossRef Medline
15. Molinaro, A., Wahlström, A., and Marschall, H. U. (2018) Role of bile acids in metabolic control. *Trends Endocrinol. Metab.* **29,** 31–41 CrossRef Medline
16. Chiang, J. Y. L., and Ferrell, J. M. (2018) Bile acid metabolism in liver pathobiology. *Gene Expr.* **18,** 71–87 CrossRef Medline
17. Shapiro, H., Kolodziejczyk, A. A., Halstuch, D., and Elinav, E. (2018) Bile acids in glucose metabolism in health and disease. *J. Exp. Med.* **215,** 383–396 CrossRef Medline
18. Schaap, F. G., Trauner, M., and Jansen, P. L. (2014) Bile acid receptors as targets for drug development. *Nat. Rev. Gastroenterol. Hepatol.* **11,** 55–67 CrossRef Medline
19. Kleiner, D. E., Brunt, E. M., Van Natta, M., Behling, C., Contos, M. J., Cummings, O. W., Ferrell, L. D., Liu, Y. C., Torbenson, M. S., Unalp-Arida, A., Yeh, M., McCullough, A. J., Sanyal, A. J., and Nonalcoholic Steatohepatitis Clinical Research Network (2005) Design and validation of a histological scoring system for nonalcoholic fatty liver disease. *Hepatology* **41,** 1313–1321 CrossRef Medline
20. Russell, K. N., Mehler, S. J., Skorupski, K. A., Baez, J. L., Shofer, F. S., and Goldschmidt, M. H. (2007) Clinical and immunohistochemical differentiation of gastrointestinal stromal tumors from leiomyosarcomas in dogs: 42 cases (1990–2003). *J. Am. Vet. Med. Assoc.* **230,** 1329–1333 CrossRef Medline
21. Lanaspa, M. A., Ishimoto, T., Li, N., Cicerchi, C., Orlicky, D. J., Ruzycki, P., Rivard, C., Inaba, S., Roncal-Jimenez, C. A., Bales, E. S., Diggle, C. P., Asipu, A., Petrash, J. M., Kosugi, T., Maruyama, S., *et al.* (2013) Endogenous fructose production and metabolism in the liver contributes to the development of metabolic syndrome. *Nat. Commun.* **4,** 2434 CrossRef Medline
22. Ursell, L. K., Clemente, J. C., Rideout, J. R., Gevers, D., Caporaso, J. G., and Knight, R. (2012) The interpersonal and intrapersonal diversity of human-associated microbiota in key body sites. *J. Allergy Clin. Immunol.* **129,** 1204–1208 CrossRef Medline
23. Liu, R., Hong, J., Xu, X., Feng, Q., Zhang, D., Gu, Y., Shi, J., Zhao, S., Liu, W., Wang, X., Xia, H., Liu, Z., Cui, B., Liang, P., Xi, L., *et al.* (2017) Gut microbiome and serum metabolome alterations in obesity and after weight-loss intervention. *Nat. Med.* **23,** 859–868 CrossRef Medline
24. Mehal, W. Z. (2013) The gordian knot of dysbiosis, obesity and NAFLD. *Nat. Rev. Gastroenterol. Hepatol.* **10,** 637–644 CrossRef Medline
25. Wieland, A., Frank, D. N., Harnke, B., and Bambha, K. (2015) Systematic review: microbial dysbiosis and nonalcoholic fatty liver disease. *Aliment. Pharmacol. Ther.* **42,** 1051–1063 CrossRef Medline
26. Boursier, J., Mueller, O., Barret, M., Machado, M., Fizanne, L., Araujo-Perez, F., Guy, C. D., Seed, P. C., Rawls, J. F., David, L. A., Hunault, G., Oberti, F., Calès, P., and Diehl, A. M. (2016) The severity of nonalcoholic fatty liver disease is associated with gut dysbiosis and shift in the metabolic function of the gut microbiota. *Hepatology* **63,** 764–775 CrossRef Medline
27. Tilg, H., Cani, P. D., and Mayer, E. A. (2016) Gut microbiome and liver diseases. *Gut.* **65,** 2035–2044 CrossRef Medline
28. Karlsson, F. H., Tremaroli, V., Nookaew, I., Bergström, G., Behre, C. J., Fagerberg, B., Nielsen, J., and Bäckhed, F. (2013) Gut metagenome in european women with normal, impaired and diabetic glucose control. *Nature* **498,** 99–103 CrossRef Medline
29. Qin, J., Li, Y., Cai, Z., Li, S., Zhu, J., Zhang, F., Liang, S., Zhang, W., Guan, Y., Shen, D., Peng, Y., Zhang, D., Jie, Z., Wu, W., Qin, Y., *et al.* (2012) A metagenome-wide association study of gut microbiota in type 2 diabetes. *Nature* **490,** 55–60 CrossRef Medline
30. Larsen, N., Vogensen, F. K., van den Berg, F. W., Nielsen, D. S., Andreasen, A. S., Pedersen, B. K., Al-Soud, W. A., Sørensen, S. J., Hansen, L. H., and Jakobsen, M. (2010) Gut microbiota in human adults with type 2 diabetes differs from non-diabetic adults. *PLoS One* **5,** e9085 CrossRef Medline
31. Utzschneider, K. M., Kratz, M., Damman, C. J., and Hullar, M. (2016) Mechanisms linking the gut microbiome and glucose metabolism. *J. Clin. Endocrinol. Metab.* **101,** 1445–1454 CrossRef Medline

32. Caussy, C., Tripathi, A., Humphrey, G., Bassirian, S., Singh, S., Faulkner, C., Bettencourt, R., Rizo, E., Richards, L., Xu, Z. Z., Downes, M. R., Evans, R. M., Brenner, D. A., Sirlin, C. B., Knight, R., *et al.* (2019) A gut microbiome signature for cirrhosis due to nonalcoholic fatty liver disease. *Nat. Commun.* **10,** 1406 CrossRef Medline
33. Kolodziejczyk, A. A., Zheng, D., Shibolet, O., and Elinav, E. (2019) The role of the microbiome in NAFLD and nash. *EMBO Mol. Med.* **11,** e9302 CrossRef Medline
34. Ponziani, F. R., Bhoori, S., Castelli, C., Putignani, L., Rivoltini, L., Del Chierico, F., Sanguinetti, M., Morelli, D., Paroni Sterbini, F., Petito, V., Reddel, S., Calvani, R., Camisaschi, C., Picca, A., Tuccitto, A., *et al.* (2019) Hepatocellular carcinoma is associated with gut microbiota profile and inflammation in nonalcoholic fatty liver disease. *Hepatology* **69,** 107–120 CrossRef Medline
35. Miele, L., Valenza, V., La Torre, G., Montalto, M., Cammarota, G., Ricci, R., Mascianà, R., Forgione, A., Gabrieli, M. L., Perotti, G., Vecchio, F. M., Rapaccini, G., Gasbarrini, G., Day, C. P., and Grieco, A. (2009) Increased intestinal permeability and tight junction alterations in nonalcoholic fatty liver disease. *Hepatology* **49,** 1877–1887 CrossRef Medline
36. Kapil, S., Duseja, A., Sharma, B. K., Singla, B., Chakraborti, A., Das, A., Ray, P., Dhiman, R. K., and Chawla, Y. (2016) Small intestinal bacterial overgrowth and Toll-like receptor signaling in patients with non-alcoholic fatty liver disease. *J. Gastroenterol. Hepatol.* **31,** 213–221 CrossRef Medline
37. Vrieze, A., Van Nood, E., Holleman, F., Salojärvi, J., Kootte, R. S., Bartelsman, J. F., Dallinga-Thie, G. M., Ackermans, M. T., Serlie, M. J., Oozeer, R., Derrien, M., Druesne, A., Van Hylckama Vlieg, J. E., Bloks, V. W., Groen, A. K., *et al.* (2012) Transfer of intestinal microbiota from lean donors increases insulin sensitivity in individuals with metabolic syndrome. *Gastroenterology* **143,** 913–916.e7 CrossRef Medline
38. Wang, J., Tang, H., Zhang, C., Zhao, Y., Derrien, M., Rocher, E., van Hylckama Vlieg, J. E., Strissel, K., Zhao, L., Obin, M., and Shen, J. (2015) Modulation of gut microbiota during probiotic-mediated attenuation of metabolic syndrome in high fat diet-fed mice. *Isme J.* **9,** 1–15 CrossRef Medline
39. Pathak, P., Xie, C., Nichols, R. G., Ferrell, J. M., Boehme, S., Krausz, K. W., Patterson, A. D., Gonzalez, F. J., and Chiang, J. Y. L. (2018) Intestine farnesoid X receptor agonist and the gut microbiota activate g-protein bile acid receptor-1 signaling to improve metabolism. *Hepatology* **68,** 1574–1588 CrossRef Medline
40. Boyer, J. L. (2013) Bile formation and secretion. *Compr. Physiol.* **3,** 1035–1078 Medline
41. Jiang, C., Xie, C., Li, F., Zhang, L., Nichols, R. G., Krausz, K. W., Cai, J., Qi, Y., Fang, Z. Z., Takahashi, S., Tanaka, N., Desai, D., Amin, S. G., Albert, I., Patterson, A. D., and Gonzalez, F. J. (2015) Intestinal farnesoid X receptor signaling promotes nonalcoholic fatty liver disease. *J. Clin. Invest.* **125,** 386–402 CrossRef Medline
42. McGettigan, B. M., McMahan, R. H., Luo, Y., Wang, X. X., Orlicky, D. J., Porsche, C., Levi, M., and Rosen, H. R. (2016) Sevelamer improves steatohepatitis, inhibits liver and intestinal farnesoid X receptor (FXR), and reverses innate immune dysregulation in a mouse model of non-alcoholic fatty liver disease. *J. Biol. Chem.* **291,** 23058–23067 CrossRef Medline
43. Turnbaugh, P. J., Ley, R. E., Mahowald, M. A., Magrini, V., Mardis, E. R., and Gordon, J. I. (2006) An obesity-associated gut microbiome with increased capacity for energy harvest. *Nature* **444,** 1027–1031 CrossRef Medline
44. Kau, A. L., Ahern, P. P., Griffin, N. W., Goodman, A. L., and Gordon, J. I. (2011) Human nutrition, the gut microbiome and the immune system. *Nature* **474,** 327–336 CrossRef Medline
45. Ley, R. E. (2010) Obesity and the human microbiome. *Curr. Opin. Gastroenterol.* **26,** 5–11 CrossRef Medline
46. Dawson, P. A., and Karpen, S. J. (2015) Intestinal transport and metabolism of bile acids. *J. Lipid Res.* **56,** 1085–1099 CrossRef Medline
47. Ridlon, J. M., Kang, D. J., Hylemon, P. B., and Bajaj, J. S. (2014) Bile acids and the gut microbiome. *Curr. Opin. Gastroenterol.* **30,** 332–338 CrossRef Medline
48. Kraus, D., Yang, Q., and Kahn, B. B. (2015) Lipid extraction from mouse feces. *Bio. Protoc.* **5,** e1375 CrossRef Medline
49. Jiang, T., Wang, X. X., Scherzer, P., Wilson, P., Tallman, J., Takahashi, H., Li, J., Iwahashi, M., Sutherland, E., Arend, L., and Levi, M. (2007) Farnesoid X receptor modulates renal lipid metabolism, fibrosis, and diabetic nephropathy. *Diabetes* **56,** 2485–2493 CrossRef Medline
50. Wang, X. X., Edelstein, M. H., Gafter, U., Qiu, L., Luo, Y., Dobrinskikh, E., Lucia, S., Adorini, L., D'Agati, V. D., Levi, J., Rosenberg, A., Kopp, J. B., Gius, D. R., Saleem, M. A., and Levi, M. (2016) G protein-coupled bile acid receptor tgr5 activation inhibits kidney disease in obesity and diabetes. *J. Am. Soc. Nephrol.* **27,** 1362–1378 CrossRef Medline
51. Lanaspa, M. A., Andres-Hernando, A., Orlicky, D. J., Cicerchi, C., Jang, C., Li, N., Milagres, T., Kuwabara, M., Wempe, M. F., Rabinowitz, J. D., Johnson, R. J., and Tolan, D. R. (2018) Ketohexokinase c blockade ameliorates fructose-induced metabolic dysfunction in fructose-sensitive mice. *J. Clin. Invest.* **128,** 2226–2238 CrossRef Medline
52. The R Development Core Team (2014) R: a language and environment for statistical computing, R Foundation for Statistical Computing
53. Jiang, C., Xie, C., Lv, Y., Li, J., Krausz, K. W., Shi, J., Brocker, C. N., Desai, D., Amin, S. G., Bisson, W. H., Liu, Y., Gavrilova, O., Patterson, A. D., and Gonzalez, F. J. (2015) Intestine-selective farnesoid X receptor inhibition improves obesity-related metabolic dysfunction. *Nat. Commun.* **6,** 10166 CrossRef Medline
54. Suhalim, J. L., Chung, C. Y., Lilledahl, M. B., Lim, R. S., Levi, M., Tromberg, B. J., and Potma, E. O. (2012) Characterization of cholesterol crystals in atherosclerotic plaques using stimulated Raman scattering and second-harmonic generation microscopy. *Biophys. J.* **102,** 1988–1995 CrossRef Medline
55. Lim, R. S., Suhalim, J. L., Miyazaki-Anzai, S., Miyazaki, M., Levi, M., Potma, E. O., and Tromberg, B. J. (2011) Identification of cholesterol crystals in plaques of atherosclerotic mice using hyperspectral cars imaging. *J. Lipid Res.* **52,** 2177–2186 CrossRef Medline
56. Lim, R. S., Kratzer, A., Barry, N. P., Miyazaki-Anzai, S., Miyazaki, M., Mantulin, W. W., Levi, M., Potma, E. O., and Tromberg, B. J. (2010) Multimodal cars microscopy determination of the impact of diet on macrophage infiltration and lipid accumulation on plaque formation in apoe-deficient mice. *J. Lipid Res.* **51,** 1729–1737 CrossRef Medline
57. Jonscher, K. R., Alfonso-Garcia, A., Suhalim, J. L., Orlicky, D. J., Potma, E. O., Ferguson, V. L., Bouxsein, M. L., Bateman, T. A., Stodieck, L. S., Levi, M., Friedman, J. E., Gridley, D. S., and Pecaut, M. J. (2016) Spaceflight activates lipotoxic pathways in mouse liver. *PLoS One* **11,** e0152877 CrossRef Medline
58. Friedman, J. E., Dobrinskikh, E., Alfonso-Garcia, A., Fast, A., Janssen, R. C., Soderborg, T. K., Anderson, A. L., Reisz, J. A., D'Alessandro, A., Frank, D. N., Robertson, C. E., de la Houssaye, B. A., Johnson, L. K., Orlicky, D. J., Wang, X. X., *et al.* (2018) Pyrroloquinoline quinone prevents developmental programming of microbial dysbiosis and macrophage polarization to attenuate liver fibrosis in offspring of obese mice. *Hepatol. Commun.* **2,** 313–328 CrossRef Medline
59. Nycz, B. T., Dominguez, S. R., Friedman, D., Hilden, J. M., Ir, D., Robertson, C. E., and Frank, D. N. (2018) Evaluation of bloodstream infections, clostridium difficile infections, and gut microbiota in pediatric oncology patients. *PLoS One* **13,** e0191232 CrossRef Medline
60. Ramakrishnan, V. R., Hauser, L. J., Feazel, L. M., Ir, D., Robertson, C. E., and Frank, D. N. (2015) Sinus microbiota varies among chronic rhinosinusitis phenotypes and predicts surgical outcome. *J. Allergy Clin. Immunol.* **136,** 334–342.e1 CrossRef Medline
61. Frank, D. N. (2009) Barcrawl and bartab: Software tools for the design and implementation of barcoded primers for highly multiplexed DNA sequencing. *BMC Bioinformatics* **10,** 362 CrossRef Medline
62. Lane, D. J., Pace, B., Olsen, G. J., Stahl, D. A., Sogin, M. L., and Pace, N. R. (1985) Rapid determination of 16s ribosomal rna sequences for phylogenetic analyses. *Proc. Natl. Acad. Sci. U.S.A.* **82,** 6955–6959 CrossRef Medline
63. Weisburg, W. G., Barns, S. M., Pelletier, D. A., and Lane, D. J. (1991) 16s ribosomal DNA amplification for phylogenetic study. *J. Bacteriol.* **173,** 697–703 CrossRef Medline
64. Ewing, B., and Green, P. (1998) Base-calling of automated sequencer traces using phred: II. Error probabilities. *Genome Res.* **8,** 186–194 CrossRef Medline

65. Edgar, R. C., Haas, B. J., Clemente, J. C., Quince, C., and Knight, R. (2011) Uchime improves sensitivity and speed of chimera detection. *Bioinformatics* **27,** 2194–2200 CrossRef Medline
66. Schloss, P. D., and Westcott, S. L. (2011) Assessing and improving methods used in operational taxonomic unit-based approaches for 16s rrna gene sequence analysis. *Appl. Environ. Microbiol.* **77,** 3219–3226 CrossRef Medline
67. Pruesse, E., Peplies, J., and Glöckner, F. O. (2012) Sina: accurate high-throughput multiple sequence alignment of ribosomal rna genes. *Bioinformatics* **28,** 1823–1829 CrossRef Medline
68. Quast, C., Pruesse, E., Yilmaz, P., Gerken, J., Schweer, T., Yarza, P., Peplies, J., and Glöckner, F. O. (2013) The silva ribosomal rna gene database project: Improved data processing and web-based tools. *Nucleic Acids Res.* **41,** D590–D596 Medline
69. Robertson, C. E., Harris, J. K., Wagner, B. D., Granger, D., Browne, K., Tatem, B., Feazel, L. M., Park, K., Pace, N. R., and Frank, D. N. (2013) Explicet: graphical user interface software for metadata-driven management, analysis and visualization of microbiome data. *Bioinformatics* **29,** 3100–3101 CrossRef Medline